Title

Spin Rectification and Electrically Controlled Spin Transport in Molecular-Ferroelectrics-Based Spin Valves

Journal

Physical Review Applied, 13(6)

ISSN

2331-7043

Authors

Yin, Yuewei

Jiang, Xuanyuan

Koten, Mark A

et al.

Publication Date

2020-06-01

DOI

10.1103/physrevapplied.13.064011

Peer reviewed

Spin Rectification and Electrically Controlled Spin Transport in Molecular-Ferroelectrics-Based Spin Valves

Yuewei Yin,[1,2] Xuanyuan Jiang,[1] Mark A. Koten,[3] Jeffrey E. Shield,[3] Xuegang Chen,[1] Yu Yun,[1] Alpha T. N'Diaye,[4] Xia Hong,[1] and Xiaoshan Xu[1,*]

[1] *Department of Physics and Astronomy, Nebraska Center for Materials and Nanoscience, University of Nebraska, Lincoln, Nebraska 68588, USA*

[2] *Hefei National Laboratory for Physical Sciences at the Microscale, Department of Physics, and CAS Key Laboratory of Strongly-Coupled Quantum Matter Physics, University of Science and Technology of China, Hefei, China*

[3] *Department of Mechanical and Materials Engineering, University of Nebraska, Lincoln, Nebraska 68588, USA*

[4] *Advanced Light Source, Lawrence Berkeley National Laboratory, Berkeley, California 94720, USA*

We report a spin-rectification effect in a spin-valve structure consisting of ferroelectric croconic acid ($C_5H_2O_5$) sandwiched between ferromagnetic electrodes $La_{0.7}Sr_{0.3}MnO_3$ and Co, which can be switched between a high-resistance (*off*) and a low-resistance (*on*) state by a poling voltage. In the *off* state, the magnetoresistance (MR) sign reverses with the measurement voltage with a 0.1-V offset, suggesting a spin-rectification behavior, while in the *on* state the MR remains negative. These observations can be understood in terms of electrically controlled interfacial energy-band alignment either from the electrostatic effect or from the interfacial redox process. The observed spin-rectification effect suggests the possibility of diodelike devices for spin-polarized current.

I. INTRODUCTION

Electrical control of spin transport is critical for developing spin-based circuitry [1–3]. The realization of this control hinges on the sensitivity of fundamental processes such as the generation and detection of spin currents to the electrical field. In multilayer structures such as spin valves, spin current can be generated and detected using ferromagnetic (FM)-nonmagnetic (NM) interfaces. Their efficiencies are determined by the interfacial spin polarizations P^s, which manifest in magnetoresistance (MR) [4]. Therefore, manipulation of P^s can be an effective method for the electrical control of spin transport.

A significant change of P^s is its sign reversal. The reversal of the P^s sign when the electrical current is reversed can be viewed as a spin-rectification effect for the FM-NM interface, which could be useful for tunable spin filtering. The spin rectification of an FM-NM interface in a spin-valve structure can be inferred from an MR sign reversal with the measurement voltage, if the P^s sign of the other FM-NM interface is unchanged, as illustrated in Fig. 1(a). Although the magnitude of the MR naturally decreases with the measurement voltage [5–11] due to, e.g., spin depolarization of hot carriers [12], MR sign reversal at low voltage, or the spin-rectification effect, has been found to be rare.

In order to realize the spin-rectification effect, in this work, we employ active band-alignment engineering in a spin-valve structure consisting of molecular ferroelectric croconic acid ($C_5H_2O_5$ or CA for abbreviation) sandwiched between ferromagnetic electrodes $La_{0.7}Sr_{0.3}MnO_3$ (LSMO) and Co. The advantage of CA [Fig. 1(b)] is its large electric polarization (25 $\mu C/cm^2$) [13] and the unique proton-transfer origin of the ferroelectricity [13–16], which enhances the electrostatic effect and minimizes the interfacial structural change. Using a poling voltage, the spin-valve structure is switched between a low-resistance (*on*) state and a high-resistance (*off*) state, in which the spin-rectification effect is observed.

II. METHODS

The $La_{0.7}Sr_{0.3}MnO_3$(15-nm) thin films are epitaxially grown on $SrTiO_3$ (001) substrate by pulsed laser deposition and magnetron sputtering, where the 0.7/0.3 composition is chosen for its robust magnetic properties [17]. The nanometer-thin film of CA is fabricated by thermal evaporation followed by the growth of SiO_2 by electron-beam (*e*-beam) evaporation. The Co(20-nm)/Al(2-nm) top electrode, with a diameter of approximately 200 μm, is grown using *e*-beam evaporation with a shadow mask. The

*xiaoshan.xu@unl.edu

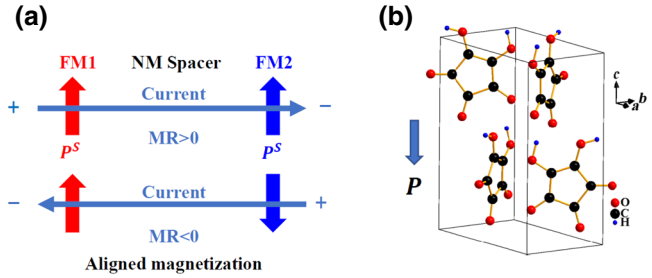

FIG. 1. (a) A schematic illustration. Upon current reversal, when the P^s sign of the FM1-NM interface remains the same, MR sign reversal suggests P^s sign reversal, or the spin-rectification effect of the FM2-NM interface. The vertical arrows indicates the spin polarization at the FM/NM boundary; the horizontal arrows indicate the current directions; the magnetization of the two FM electrodes is always aligned. (b) The crystal structure of CA, where the electrical polarization is along the *c* axis. *P* indicates electric polarization.

growth of the CA, SiO_2, Co, and Al layers is carried out in high vacuum with an EvoVac system from Angstrom Engineering, at −30 °C substrate temperature to optimize the CA-layer morphology and to minimize the interlayer diffusion [18]. The cross-section STO/LSMO/CA/SiO_2/Co structure is characterized by high-resolution transmission electron microscopy (HRTEM) using a FEI Tecnai Osiris S/TEM operating at 200 kV. Electron-transparent samples are produced using standard lift-out procedures on a FEI Helios Nanolab 660.

Polarization-hysteresis-loop measurements and piezo-response-force microscopy are used to characterize the ferroelectric properties of the CA film, as demonstrated by our previous study [18]. Electrical and magnetotransport measurements are performed with a Keithley 2450 SourceMeter, using a four-probe method in a Janis cryostat with a 0.5-T electromagnet. The positive bias corresponds to current flow from the top Co to the bottom LSMO electrode. Constant-voltage biases are used and an automatic feedback loop is turned on to ensure a constant voltage drop across the junction through the voltage leads. All the resistances are measured under the "measurement voltage" V_{meas}; a pulsed (20-ms duration) "poling voltage," V_{pole}, is applied on the junction to change the resistance states, which are measured with a low V_{meas} right after V_{pole}.

The temperature and magnetic-field dependencies of the magnetization are measured using a superconducting quantum interference device (SQUID) magnetometer, with the field along the in-plane direction. X-ray absorption spectroscopy (XAS) of the Co *L* edge measurements and x-ray magnetic circular dichroism (XMCD) are performed with normal incidence at the bend-magnet beamline 6.3.1 in the Advanced Light Source at the Lawrence Berkeley National Laboratory.

III. RESULTS

A. Spin-valve structure

Figure 2(a) shows schematically the structure of the LSMO/CA/SiO_2/Co spin valve. The HRTEM image of the cross-section structure is shown in Figs. 2(b)–2(d), confirming the desired thicknesses of the different layers. More importantly, there is no visible diffusion of Co into the CA layer, indicating the effectiveness of the SiO_2 layer as a diffusion barrier.

B. Electroresistance

As indicated by the structure in Fig. 2(a), a voltage is applied to the Co top electrode and the LSMO bottom electrode is always grounded. Figure 3(a) shows the typical current-voltage (*I*-*V*) characteristics measured at 30 K with bipolar switching between a high-resistance (*on*) state and a low-resistance (*off*) state. The weak temperature dependence of the resistance suggests the tunneling nature of the conduction (see Fig. S1 in the Supplemental Material [19]). The electroresistance, defined as ER ≡ R_{off}/R_{on}, increases with decreasing V_{meas} and reaches 3500% close to zero V_{meas} (see Fig. S1 in the Supplemental Material [19]), where R_{off} and R_{on} are the resistances for the *off* and *on* states, respectively.

To further demonstrate the ER behavior, we apply a sequence (2.5 V → −2.5 V → 2.5 V) of pulsed (20-ms duration) poling voltages (V_{pole}) on the junction to

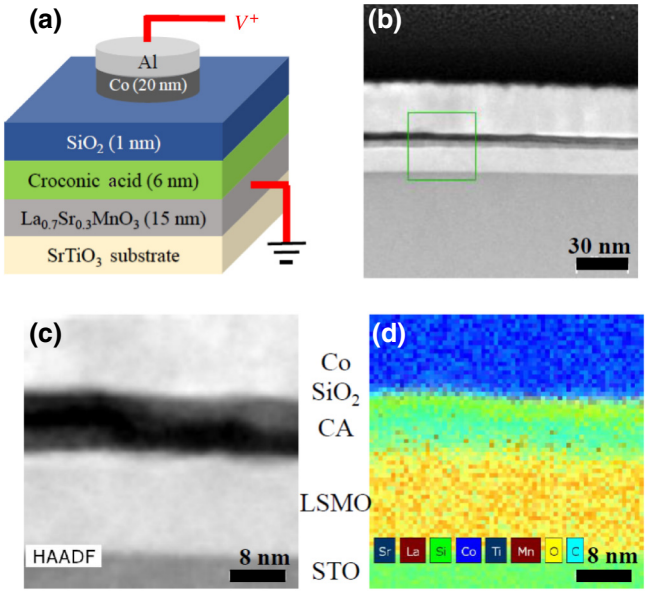

FIG. 2. (a) The schematics of the LSMO/CA/SiO_2/Co spin-valve structure. (b)–(d) Transmission electron microscopy images on the cross section of a STO/LSMO/CA/SiO_2/Co structure. (b) A high-angle annular dark-field (HAADF) image. An enlarged view of the area in the box in (b) is shown in (c). (d) Element mapping of the same area as shown in (c).

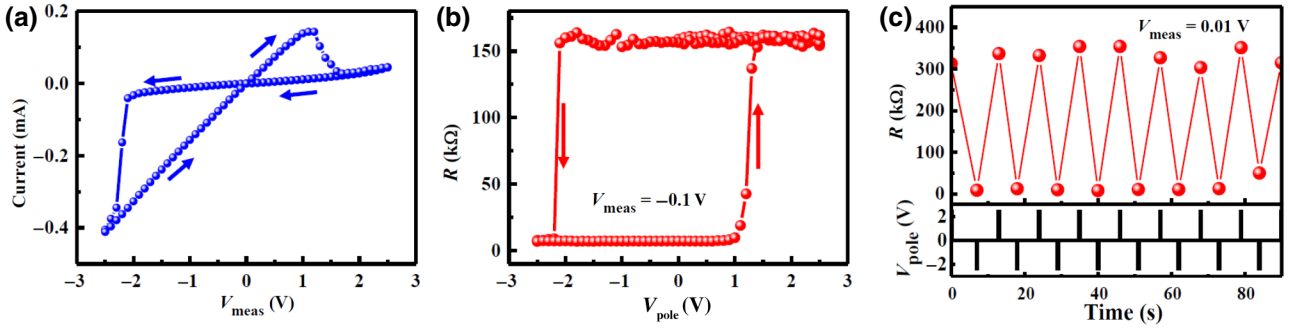

FIG. 3. (a) The current versus voltage (V_{meas}) characteristics. (b) The resistances as a function of V_{pole} measured at $V_{meas} = -0.01$ V. (c) The typical resistance switching between the *on* and *off* states measured at $V_{meas} = -0.1$ V, after applying a V_{pole} of +2.5 V or −2.5 V. The measurements in (a)–(c) are carried out at 30 K.

change the resistance state, which is measured at a constant $V_{meas} = -0.1$ V right after the pulse; the measured resistance as a function of V_{pole} is shown in Fig. 3(b). Consistent with the I-V measurement in Fig. 3(a), the junction shows low-resistance states after negative $V_{pole} < -2.3$ V and high-resistance states after positive $V_{pole} > 1.5$ V. To confirm the reversible switching between the *on* and *off* states, measurements are performed by applying +2.5 V and −2.5 V pulses back and forth; the reproducibility is demonstrated in Fig. 3(c).

C. Magnetoresistance

Figures 4(a) and 4(b) show representative curves of the resistance versus the magnetic field $R(H)$ for the junction in the *on* and *off* states. Typical $R(H)$ curves with a rapid resistance change at the coercive fields of LSMO and Co electrodes are observed. Here, the switching at the smaller (larger) magnetic fields corresponds to the magnetization reversal in LSMO (Co) electrode, consistent with the magnetometry measurements (see Fig. S2 in the Supplemental Material [19]).

The behavior of the MR for the *on* and *off* states differs dramatically; here, MR $\equiv (R_{AP} - R_P)/R_P$, where R_P and R_{AP} are the resistance when the magnetization of the FM electrodes are parallel and antiparallel, respectively. In the *on* state, the MR is negative at both $V_{meas} = -1$ and 1 V, as shown in Figs. 4(a) and 4(b), respectively. The voltage dependence of the MR, i.e., MR(V_{meas}), is shown in Fig. 4(c); negative MR is observed regardless of the sign of V_{meas} in the *on* state. This is typical for magnetic tunnel junctions using two ferromagnetic electrodes with opposite P^s signs [20,21]. The magnitude of the MR, up to 12.5%, decreases with an increasing $|V_{meas}|$ in the *on* state, consistent with the mechanism of spin depolarization of hot electrons [12]. In contrast, in the *off* state, the MR at $V_{meas} = -1$ and 1 V has opposite signs, as shown in Fig. 4(a) and 4(b), respectively. In fact, as shown in Fig. 4(c), the MR is essentially positive at negative V_{meas} and negative at positive V_{meas} with a 0.1 V offset in the *off* state. This is different from the V_{meas}-independent MR sign in previously reported organic spin valve [22].

The dramatic difference between the MR(V_{meas}) values of the *on* and *off* states is also observed at higher temperatures, e.g., 100 K, as shown in Fig. 5(a). In the *off* state, the MR sign reverses at around $V_{meas} = -0.1$ V, which is

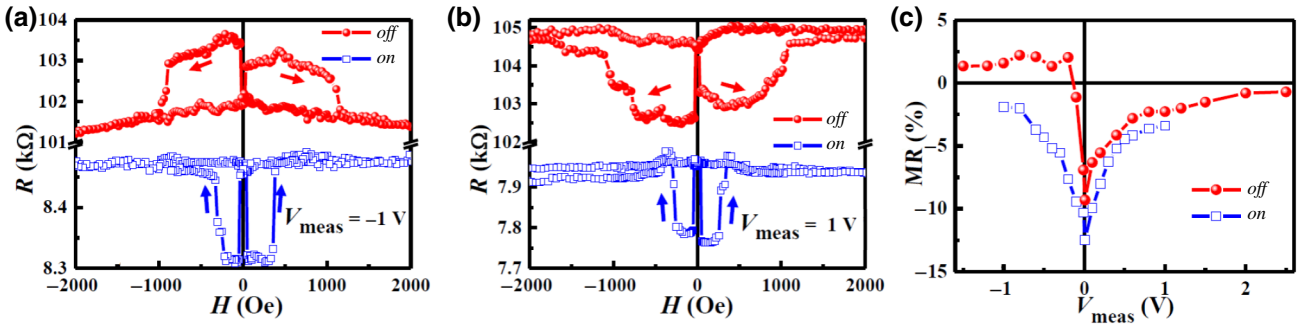

FIG. 4. The MR under (a) $V_{meas} = -1$ V and (b) $V_{meas} = +1$ V after applying $V_{pole} = +2.5$ V and $V_{pole} = -2.5$ V, respectively. The arrows indicate the measurement sequence. (c) The MR as a function of V_{meas} for both the *on* (low resistance) and *off* (high resistance) states. The measurements are carried out at 30 K, with an in-plane magnetic field.

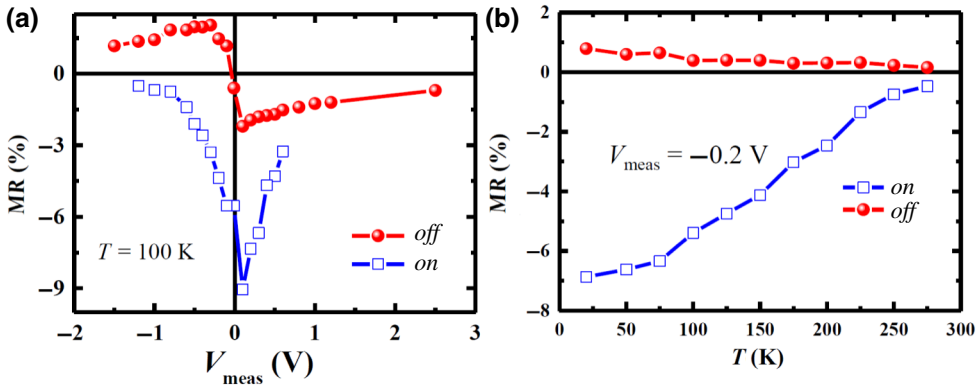

FIG. 5. (a) The bias-dependent MR at 100 K for the *on* and the *off* states. (b) The temperature-dependent MR for the *on* and the *off* states. The magnetic field is in the film plane.

similar to that at 30 K, while in the *on* state, the MR sign is also always negative, with a peak value about −9.1%. The magnitude of the MR in general decreases with temperature and vanishes at around room temperature, as shown in Fig. 5(b), measured in a different device.

D. Spin-rectification effect and theoretical model

The direct effect of V_{pole} on the resistance of the junction, i.e., ER, can be understood with the mechanism of tunnel ferroelectric resistance, which has been predicted theoretically in a $SrRuO_3/BaTiO_3/SrTiO_3/SrRuO_3$ heterojunction [23]. The surface charge σ_P of a ferroelectric layer sandwiched between electrodes is normally screened at the ferroelectric-electrode interfaces. More specifically, in short-circuit conditions, the screening charge is $\sigma_S = \sigma_P d_F/(\delta_1 + \delta_2 + d_F)$, where d_F is the thickness of the ferroelectric layer and δ_1 and δ_2 are the screening lengths of the two electrodes [24]. When $\delta_1 + \delta_2 \ll d_F$, which is the case for typical metals, σ_S approaches σ_P, meaning a complete screening. The change of vacuum potential in the ferroelectric layer can be written as $\Delta V_F = d_F(\sigma_P - \sigma_S)/\varepsilon_0$ [24], which vanishes when σ_S approaches σ_P, where ε_0 is the vacuum permittivity. With the dielectric layer SiO_2 inserted, the screening charge follows $\sigma_S = \sigma_P d_F/(\delta_1 + \delta_2 + d_F + d_D/\varepsilon_D)$, where d_D and ε_D are the thickness and the relative dielectric constant of the SiO_2 layer. If $\delta_1 + \delta_2 + d_D/\varepsilon_D$ is comparable to d_F, σ_S is substantially reduced and ΔV_F becomes nonzero. The change of vacuum potential affects the energy landscape of the tunnel junction and, most importantly, the effective height of the tunnel barrier. As illustrated in Fig. 6(a) (see also Appendix A), the overall vacuum level shifts up (down) when the CA polarization points "down" ("up") toward the LSMO (Co), which is expected to raise (lower) the tunnel barrier and cause higher (lower) resistance; this is consistent with the observation in the LSMO/CA/SiO_2/Co junction in Fig. 3: a positive (negative) poling voltage leads to the *off* (*on*) state.

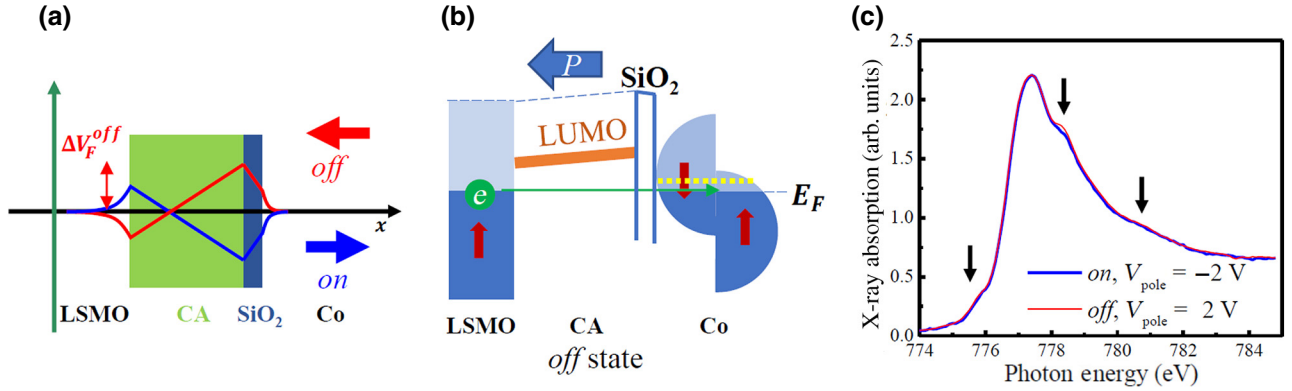

FIG. 6. (a) The schematics of the electronic vacuum potential for both the *on* and *off* states; the arrows indicate the polarization direction of CA. ΔV_F^{off} is the change of vacuum potential in the ferroelectric layer in the *off* state. (b) An energy diagram illustrating the shift of the Fermi energy in interfacial Co at zero measurement voltage V_{meas} due to the electrostatic effect in the *off* state. The vertical thick arrow indicates the magnetization directions. The horizontal thick arrows indicate the electric polarization. The horizontal (green) arrow indicates the tunneling process. The (yellow) dashed lines indicate the bulk Fermi-energy level of Co. (c) X-ray absorption spectra of the Co L_3 edge for the *on* and *off* states. The arrows indicate features from Co^{2+}. The measurements are carried out at 80 K.

To understand the effect of V_{pole} on MR(V_{meas}), we first note that MR(V_{meas}) depends on the energy landscape of the LSMO/CA/SiO_2/Co junction. For spin-conserved tunneling across the junction, according to Julliere's model [25], the sign of the MR is determined by the product $P^s_{LSMO}P^s_{Co}$. Previous work has demonstrated that, in a LSMO/$SrTiO_3$/Co spin valve, the energy and spin polarization of electrons participating in the charge transfer depend on V_{meas}, causing the dependence of the effective P^s and the MR on V_{meas} and even a MR sign change [20,21]. While the spin polarization of the LSMO interface, (P^s_{LSMO}), is believed to remain positive around the Fermi level due to the large gap between the Fermi energy and the minority band [17,26,27], the spin polarization of the Co interface (P^s_{Co}) changes dramatically with the energy (see also Appendix B). So, it is concluded that the MR(V_{meas}) relation in the LSMO/$SrTiO_3$/Co spin valve comes mostly from the dependence of P^s_{Co} on V_{meas} [20,21]; Unfortunately, the V_{meas} needed for the MR sign change is too large (approximately 1 V) in the LSMO/$SrTiO_3$/Co spin valve. In contrast, in this work, in the *off* state of the LSMO/CA/SiO_2/Co junction, the MR sign reversal occurs at much lower V_{meas} (approximately 0.1 V). Therefore, assuming that the P^s_{LSMO} sign remains the same, in the *off* state of the LSMO/CA/SiO_2/Co spin valve reported here, P^s_{Co} basically changes sign when V_{meas} changes sign, i.e., the Co interface exhibits the spin-rectification effect, as illustrated in Fig. 1(a).

Following the mechanism of spin-conserved tunneling [20,21], if the Fermi energy of Co is shifted relative to the density of states, the MR(V_{meas}) relation will be shifted accordingly. In particular, to have a sign change of the MR around zero V_{meas} in the *off* state, it is required that P^s_{Co} reverses sign around the Fermi energy, which means a down-shift of the Fermi energy relative to the density of states, since the minority spin dominates at the Fermi energy in bulk Co. The measured $R(H)$ relation [Figs. 4(a) and 4(b)] indicates that the coercivity of the Co is clearly larger (smaller) when the junction is in the *off* (*on*) state, suggesting a change of electronic structure. In contrast, the magnetic hysteresis loop of Co measured using a local XMCD probe shows less obvious change between the *on* and *off* states (see Fig. S3 in the Supplemental Material [19]), suggesting that the change occurs at the interface. Here, we propose that the down-shift of the Fermi energy relative to the density of state for the interfacial Co in the *off* state is caused by the electrostatic effect of the ferroelectric polarization, as illustrated in Fig. 6(b) (see also Appendix C).

As depicted in Fig. 6(b), the electric polarization of a ferroelectric material may shift the vacuum potential across the junction. In open-circuit conditions, this vacuum potential shift causes a shift of the density of states of Co. In short-circuit conditions (zero V_{meas}), to unify the Fermi energy of the whole junction, a charge accumulation or depletion and a shift in the Fermi energy relative to the density of states in the interfacial Co occurs. For example, as illustrated in Fig. 6(b), in the *off* state, the polarization pointing toward the LSMO causes electron depletion in the Co, raises its density of states, and down-shifts its Fermi energy at zero V_{meas} (see also Appendix C). The order of magnitude of the energy shift can be estimated using $\Phi = \sigma_S\delta/\varepsilon_0 \approx \sigma_P\delta/\varepsilon_0 \sim 1$ V (see also Appendix A), where $\sigma_P \sim 10\ \mu C/cm^2$ and $\delta \sim 1$ Å are assumed; this is in reasonable agreement with the expected energy shift considering the V_{meas} (approximately 1 V) needed for the MR sign change in the LSMO/STO/Co junction reported previously [20,21].

To confirm the possible depletion of electrons in Co for the *off* state, we carry out an x-ray absorption spectroscopy study on the Co L edge at 80 K. As shown in Fig. 6(c), the depletion of electrons in Co for the *off* state relative to that for the *on* state is observed: the spectrum for Co in the *off* state shows a larger signature of Co^{2+} than that for the *on* state [28] (see Fig. S3 in the Supplemental Material [19]).

IV. DISCUSSION

The above proposed explanation is based on the electrostatic effect of a ferroelectric interface on spin transport [29–33]. The ferroelectric interface can significantly impact the spin transport by altering the interfacial crystal and electronic structures [22,34–40] or by changing the energy-band alignment due to the electrostatic effect of the polarization [24,31,41,42]. Due to the weak organic-inorganic interaction, the electrostatic effect is expected to be more important in spin valves with organic ferroelectric spacers. Following this idea, spin valves with an organic ferroelectric spacer poly(vinylidene fluoride) (PVDF) have previously been studied in LSMO/PVDF/Co junctions [22]. However, instead of the electrostatic effect, the significant change in the interfacial structure of PVDF from H termination to F termination due to the rotation of polymer chains is found to cause the change in the interfacial spin polarization after the reversal of the ferroelectric polarization [22]. The idea of minimizing the structural effect at the ferroelectric interface has previously been examined in LSMO/PZT ($PbZr_{0.2}Ti_{0.8}O_3$)/Alq_3/Co spin valves, where Alq_3, short for tris-(8-hydroxyquinoline) aluminum [31], has been inserted between the ferroelectric PZT spacer and the magnetic electrode Co. On the other hand, in this structure, a large shift in the Co interfacial Fermi energy relative to its density of state is not expected, because the Co is separated from the PZT by a thick (approximately 50-nm) Alq_3 layer.

The benefit of using organic ferroelectric CA is that its small interfacial structural change and large electric polarization (25 $\mu C/cm^2$) [13] due to the proton-transfer origin of ferroelectricity [13–16], plus the weak interactions at the

organic-inorganic interfaces, are expected to minimize the structural effect and promote the electrostatic effect. The results of this work indeed provide evidence of voltage-controlled energy-band alignment, which is the expected electrostatic effect of the polarization reversal.

We note that it is also possible that the down-shift of the Fermi energy relative to the density of state for the interfacial Co in the *off* state of the junction is caused by the redox effect of Co (see also Appendix C). In principle, the oxygen vacancy (V_O^+) in SiO_2 may migrate when the poling voltage (V_{pole}) is applied. The *on* state results from a negative V_{pole}, which moves the oxygen vacancy toward the Co and reduces the Co. In contrast, the *off* state results from a positive V_{pole}, which moves the oxygen vacancy away from the Co and causes oxidation of Co at the interface. In the *off* state, the interfacial Co layer may be viewed as depleted in electrons; correspondingly, the Fermi energy is shifted downward, which may shift the MR(V_{meas}) relation and causes reversal of the MR sign around zero V_{meas}.

Whether the Fermi-energy shift is caused by the ferroelectric electrostatic effect or by the Co redox effect, it appears that the energy-landscape engineering is the key to tuning the interfacial spin polarization P^s. This mechanism appears to be a viable route to adjust MR(V_{meas}) to generate the spin-rectification effect, which could be crucial for the design of spintronics devices, similar to the role of charge-current rectification in modern semiconductor electronics.

V. CONCLUSION

In summary, we demonstrate the voltage control of the spin transport in the LSMO/CA/SiO_2/Co spin valves. Both the ER effect and the MR effect are obtained and the MR sign can be tuned not only by the poling voltage but also by the measurement voltage. The MR(V_{meas}) relation in the *off* state suggests the spin-rectification effect at the Co interface. These observations are consistent with the mechanism of voltage-tunable interfacial energy-band alignment that may result from the electrostatic effect of the ferroelectric polarization or the redox effect of the Co electrode. These results suggest the importance of energy-band alignment in spin transport across spin valves, confirm the advantage of organic spintronics using a molecular semiconductor as the barrier in spin valves, and reveal an intriguing spin-rectification behavior that is promising for future functionalities.

ACKNOWLEDGMENTS

This research was primarily supported by the U.S. Department of Energy (DOE), Office of Science, Basic Energy Sciences (BES), under Award No. DE-SC0019173 (device fabrication, transport measurements, magnetometry, x-ray spectroscopy, and modeling). Additional support was from the National Science Foundation (NSF) under Grant No. DMR-1420645 (electron microscopy), from NSF under Grant No. DMR-1710461 (oxide film growth), from National Natural Science Foundation of China (NSFC) under Grant No. 51790491 and National Key R&D Program of China (NKRDPC) under Grant No. 2019YFA0307900 (data analysis, manuscript drafting and revision). The use of the Advanced Light Source was supported by the U.S. Department of Energy, Office of Science, Office of Basic Energy Sciences under Contract No. DE-AC02-05CH11231. The research was performed in part in the Nebraska Nanoscale Facility: National Nanotechnology Coordinated Infrastructure and the Nebraska Center for Materials and Nanoscience, which are supported by the NSF under Grant No. ECCS-1542182, and the Nebraska Research Initiative.

APPENDIX A: ENERGY-BAND STRUCTURE

When there is a ferroelectric (FE) layer in space, the vacuum electric potential will be changed due to the polarization of the FE layer, which can be written as $\Delta V_F = d_F \sigma P/\varepsilon_0$, where d_F and σ_P are the thickness and surface charge of the ferroelectric layer and ε_0 is the vacuum permittivity. When the ferroelectric layer is sandwiched by two metal layers (M1 and M2), there is charge accumulation at the FE-M1 and FE-M2 interfaces, or screening charges, which reduces the vacuum potential change in the FE layer. In short-circuit conditions, where the Fermi levels of M1 and M2 are the same, the electric potential in M1 and M2 can be written as $\Phi_1 = \sigma_S \delta_1 \exp(x/\delta_1)/\varepsilon_0$ and $\Phi_2 = -\sigma_S \delta_2 \exp[-(x - d_F)/\delta_2]/\varepsilon_0$, respectively, where δ_1 and δ_2 are the screening lengths of M1 and M2 and σ_S is the screening charge. The vacuum potential change in the FE layer is reduced to $\Delta V_F = d_F(\sigma_P - \sigma_S)/\varepsilon_0$. Using this relation and the expressions for Φ_1 and Φ_2 and solving $\Phi_1(0) - \Phi_2(d_F) = \Delta V_F$, one finds that $\sigma_S = \sigma_P d_F/[\delta_1 + \delta_2 + d_F]$. The corresponding spatial distributions of the electric charge and the vacuum potential are illustrated in Figs. 7(a) and 7(b). If $\delta_1 + \delta_2 \ll d_F$, which is the case for typical metals, σ_S is close to σ_F, suggesting complete screening.

When a dielectric (DE) layer is inserted between FE and M2, the total vacuum potential change across the DE layer is $\Delta V_D = -d_D \sigma_S/(\varepsilon_0 \varepsilon_D)$, where the relative dielectric constant of the dielectric layer is ε_D. The electric potential in M1 and M2 can be rewritten as $\Phi_1 = \sigma_S \delta_1 \exp(x/\delta_1)/\varepsilon_0$ and $\Phi_2 = -\sigma_S \delta_2 \exp[-(x - d_F - d_D)/\delta_2]/\varepsilon_0$, respectively. Solving $\Phi_1(0) - \Phi_2(d_F + d_D) = \Delta V_F + \Delta V_D$, one finds that $\sigma_S = \sigma_P d_F/[\delta_1 + \delta_2 + d_F + d_D/\varepsilon_D]$. If d_D/ε_D is comparable to $\delta_1 + \delta_2 + d_F$, σ_S is reduced with respect to the case in which there is no dielectric layer; ΔV_F is then enhanced. The corresponding spatial distributions of the electric charge and the vacuum potential are illustrated in Figs. 7(c) and 7(d).

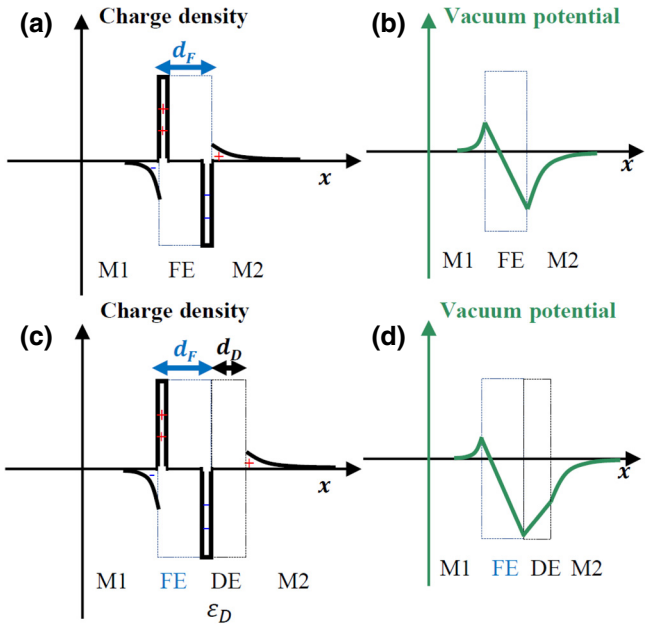

FIG. 7. The charge distribution and the vacuum potential. (a) The charge distribution of a metal (M1)/ferroelectric (FE)/metal (M2) junction. The thickness of the ferroelectric layer is d_F. (b) The vacuum electric potential of the M1/FE/M2 junction. (c) The charge distribution of a M1/FE/DE/M2 junction, where DE denotes a dielectric layer of thickness d_D. The relative dielectric constant of the DE layers is ε_D. (d) The vacuum electric potential distribution of the M1/FE/DE/M2 junction.

The energy diagram in Fig. 7 can obviously be tuned when the ferroelectric polarization is changed. Following this idea, the schematic energy diagrams of the LSMO/CA/SiO_2/Co structure are displayed in Fig. 8 for both the *off* and *on* states corresponding to two different polarization states of the CA layer. The finite screening lengths of the electrodes are ignored here to highlight the effect of the dielectric layer, SiO_2. Figure 6(a) shows

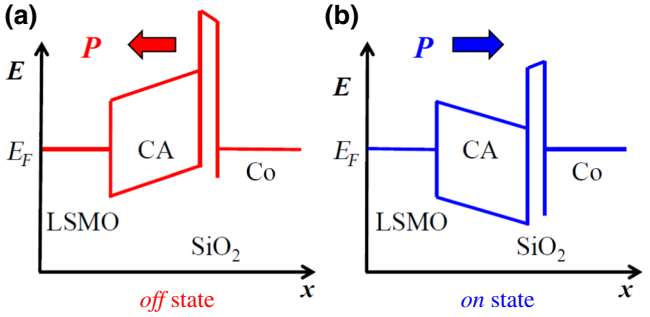

FIG. 8. The band structure of the spin valve. A schematic illustration of the energy diagram of the LSMO/CA/SiO_2/Co structure in the *off* (a) and *on* (b) states. The horizontal thick arrows indicate the electric polarization. The shifts of the energy levels are due to the vacuum level change, as illustrated in Fig. 7.

the more complete picture, taking the screening length of the electrodes into consideration.

APPENDIX B: SPIN POLARIZATION AND MAGNETORESISTANCE

For spin-polarized (ferromagnetic) materials, at the energy of electron transfer, one can define the proportion of the density of states the spin of which is parallel (antiparallel) to the magnetization as $\alpha_\uparrow$ ($\alpha_\downarrow$). The transition probability is then proportional to $\alpha_{\uparrow 1}\,\alpha_{\uparrow 2} + \alpha_{\downarrow 1}\,\alpha_{\downarrow 2}$, where the indices 1 and 2 represent the two electrodes, this being the assumption of the Julliere model. It follows that the magnetoresistance is $(R_{\rm AP} - R_{\rm P})/R_{\rm AP} = (4\alpha_{\uparrow 1}\alpha_{\uparrow 2} - 2\alpha_{\uparrow 1} - 2\alpha_{\uparrow 2} + 1)/(2\alpha_{\uparrow 1}\alpha_{\uparrow 2} - \alpha_{\uparrow 1} - \alpha_{\uparrow 2} + 1)$, where $R_{\rm P}$ and $R_{\rm AP}$ are the resistance when the magnetization are parallel and antiparallel, respectively. Defining the spin polarization $P \equiv \alpha_\uparrow - \alpha_\downarrow$, one has $(R_{\rm AP} - R_{\rm P})/R_{\rm AP} = 2P_1P_2/(1 + P_1P_2)$. Note that $0 \le \alpha \le 1$ and $-1 \le P \le 1$. Obviously, the sign of the magnetoresistance is determined by the product P_1P_2. If the spin polarization of two electrodes at the Fermi level is the same, a normal magnetoresistance, i.e., higher resistance when the magnetization is antiparallel, is expected. Otherwise, one expects an inverse magnetoresistance.

Figure 9 shows a scenario of electron transfer through a junction via quantum tunneling, where LSMO and Co are the two electrodes. Under zero $V_{\rm meas}$, the tunneling only occurs at the Fermi energy. Therefore, the sign of the magnetoresistance is determined by the $P_{\rm LMSO}P_{\rm Co}$ at the Fermi energy. For bulk LSMO, $P_{\rm LMSO} > 0$ and $P_{\rm Co} < 0$ at the Fermi level. Therefore, typically, an inverse magnetoresistance is observed. Following De Teresa *et al.* [20,21], when a bias voltage is applied, quantum tunneling occurs over the range of energy indicated in Fig. 9(a). Depending

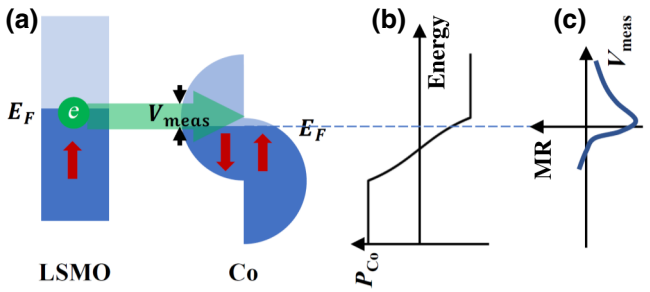

FIG. 9. The relation between the energy landscape and the MR($V_{\rm meas}$) function. (a) The energy diagram of a junction with LSMO and Co as the two ferromagnetic electrodes under a voltage $V_{\rm means}$. The vertical red arrows indicate the spin polarization. The horizontal green arrow indicates the band of energy where electrons may tunnel from LSMO to Co. (b) A schematic of the spin polarization $P_{\rm Co}$ as a function of the energy for bulk Co. (c) The MR($V_{\rm meas}$) function corresponding to the energy landscape in (a) and the spin polarization in (b).

on the bias voltage, this energy range may cover electrons with spin polarizations of different signs, which may affect the magnetoresistance. It is generally believed that around the Fermi energy, $P_{\mathrm{LMSO}} > 0$. In contrast, P_{Co} changes dramatically with the energy, as illustrated in Fig. 9(b). Therefore, by varying V_{meas}, both the positive and negative parts of the spin polarization of Co can contribute to the magnetoresistance, causing the bias dependence of the magnetoresistance or the function MR(V_{meas}), as illustrated in Fig. 9(c). In fact, a sign change of the magnetoresistance has been observed experimentally at high bias in a LSMO/STO/Co junction [20,21].

Two points are worth noting.

(1) At high bias voltage, the hot electrons are expected to be less spin polarized [12]. Therefore, in the MR(V_{meas}) function, the magnetoresistance tends to have a maximum close to zero bias.

(2) If, somehow, the Fermi energy of the Co at the interface is displaced, the MR(V_{meas}) function is expected to shift. In particular, if the Fermi energy is moved down, a sign reversal of the MR(V_{meas}) function close to zero V_{meas} is possible.

APPENDIX C: TWO MECHANISMS FOR SHIFTING THE FERMI ENERGY OF Co

1. Electrostatic effect of polarization

As shown in Fig. 10, a ferroelectric material changes the vacuum potential due to the electric polarization and the surface charge. There is charge accumulation and depletion at the FE-metal interface, where the state at the Fermi energy is not the state at the Fermi energy in bulk material. In particular, the following apply. (I) When the polarization is pointing to the Co, or the *on* state, there is accumulation of electrons in the Co at the Co/SiO_2/CA interface. Therefore, the Fermi energy is pushed up relative to the bulk density of state. (II) When the polarization is pointing to the LSMO, or the *off* state, there is depletion of electrons in

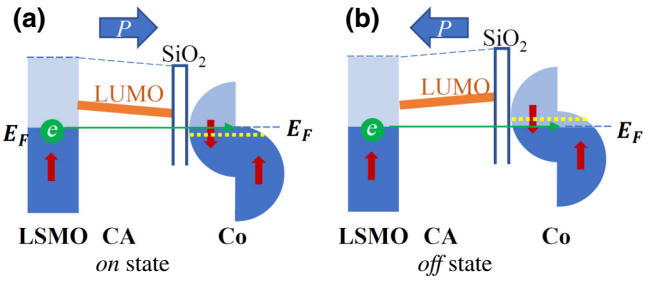

FIG. 10. Ferroelectric-polarization-reversal-induced Fermi-energy shifting in Co. (a),(b) The energy diagrams of the *on* and *off* states, respectively, where the horizontal green arrows indicate the electron-tunneling process. The yellow dashed lines represent the position of the bulk Fermi energy.

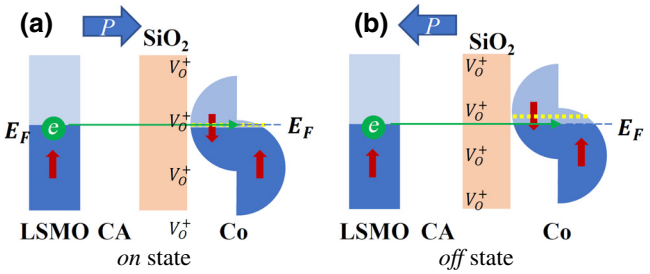

FIG. 11. Redox-process-induced Fermi-energy shifting in Co. (a) The *on* state, where the oxygen vacancy (V_O^+) is close to the Co and reduces the interfacial Co to the metallic state. (b) The *off* state, where the oxygen vacancy (V_O^+) is distant from the Co, the Co gets oxidized (e.g., to Co^{2+}), and the Fermi energy is shifted downward relative to the bulk density of states. The horizontal green arrows indicate the electron-tunneling process. The dashed yellow lines represent the position of the bulk Fermi energy at which the spin polarization is negative.

the Co at the Co/SiO_2/CA interface. Therefore, the Fermi energy is pushed down relative to the bulk density of state.

2. Redox process

In principle, the oxygen vacancy (V_O^+) in SiO_2 migrates when the poling voltage (V_{pole}) is applied. As illustrated in Fig. 11, a $V_{\mathrm{pole}} < 0$ results in the *on* state, where the oxygen vacancy migrates toward the Co and reduces the Co. The Fermi energy should remain close to the bulk level. In contrast, a $V_{\mathrm{pole}} > 0$ results in the *off* state, where the oxygen vacancy migrates away from the Co. The Co at the interface gets oxidized (e.g., to Co^{2+}), which is corroborated by the XAS study in Fig. 6(c). Here, the Co layer can be viewed as depleted in electrons; correspondingly, the Fermi energy is shifted downward.

[1] J. Sinova, S. O. Valenzuela, J. Wunderlich, C. H. Back, and T. Jungwirth, Spin Hall effects, Rev. Mod. Phys. **87**, 1213 (2015).

[2] I. Žutić, J. Fabian, and S. Das Sarma, Spintronics: Fundamentals and applications, Rev. Mod. Phys. **76**, 323 (2004).

[3] J. Wunderlich, B.-G. Park, A. C. Irvine, L. P. Zarbo, E. Rozkotova, P. Nemec, V. Novak, J. Sinova, and T. Jungwirth, Spin Hall effect transistor, Science **330**, 1801 (2010).

[4] S. Sanvito, The rise of spinterface science, Nat. Phys. **6**, 562 (2010).

[5] Z. H. Xiong, D. Wu, Z. Valy Vardeny, and J. Shi, Giant magnetoresistance in organic spin-valves, Nature **427**, 821 (2004).

[6] F. Wang and Z. V. Vardeny, Organic spin valves: The first organic spintronics devices, J. Mater. Chem. **19**, 1685 (2009).

[7] V. A. Dediu, L. E. Hueso, I. Bergenti, and C. Taliani, Spin routes in organic semiconductors, Nat. Mater. **8**, 707 (2009).

[8] F. Wang and Z. V. Vardeny, Recent advances in organic spin-valve devices, Synth. Met. **160**, 210 (2010).

[9] R. Geng, T. T. Daugherty, K. Do, H. M. Luong, and T. D. Nguyen, A review on organic spintronic materials and devices: II. Magnetoresistance in organic spin valves and spin organic light emitting diodes, J. Sci. Adv. Mater. Devices **1**, 256 (2016).

[10] J. Devkota, R. Geng, R. C. Subedi, and T. D. Nguyen, Organic spin valves: A review, Adv. Funct. Mater. **26**, 3881 (2016).

[11] H.-J. Jang and C. A. Richter, Organic spin-valves and beyond: Spin injection and transport in organic semiconductors and the effect of interfacial engineering, Adv. Mater. **29**, 1602739 (2017).

[12] S. O. Valenzuela, D. J. Monsma, C. M. Marcus, V. Narayanamurti, and M. Tinkham, Spin Polarized Tunneling at Finite Bias, Phys. Rev. Lett. **94**, 196601 (2005).

[13] S. Horiuchi, Y. Tokunaga, G. Giovannetti, S. Picozzi, H. Itoh, R. Shimano, R. Kumai, and Y. Tokura, Above-room-temperature ferroelectricity in a single-component molecular crystal, Nature **463**, 789 (2010).

[14] S. Horiuchi, R. Kumai, and Y. Tokura, Hydrogen-bonding molecular chains for high-temperature ferroelectricity, Adv. Mater. **23**, 2098 (2011).

[15] S. Horiuchi, F. Kagawa, K. Hatahara, K. Kobayashi, R. Kumai, Y. Murakami, and Y. Tokura, Above-room-temperature ferroelectricity and antiferroelectricity in benzimidazoles, Nat. Commun. **3**, 1308 (2012).

[16] Y. Noda, T. Yamada, K. Kobayashi, R. Kumai, S. Horiuchi, F. Kagawa, and T. Hasegawa, Few-volt operation of printed organic ferroelectric capacitor, Adv. Mater. **27**, 6475 (2015).

[17] E. Dagotto, T. Hotta, and A. Moreo, Colossal magnetoresistant materials: The key role of phase separation, Phys. Rep. **344**, 1 (2001).

[18] X. Jiang, H. Lu, Y. Yin, X. Zhang, X. Wang, L. Yu, Z. Ahmadi, P. S. Costa, A. D. Dichiara, X. Cheng, A. Gruverman, A. Enders, and X. Xu, Room temperature ferroelectricity in continuous croconic acid thin films, Appl. Phys. Lett. **109**, 102902 (2016).

[19] See the Supplemental Material at http://link.aps.org/supplemental/10.1103/PhysRevApplied.13.064011 for the experimental details, the V_{meas}-dependent electroresistance (ER), the magnetoresistance (MR), and the x-ray absorption study on the Co electronic structure.

[20] J. De Teresa, A. Barthélémy, A. Fert, J. Contour, R. Lyonnet, F. Montaigne, P. Seneor, and A. Vaurés, Inverse Tunnel Magnetoresistance in $Co/SrTiO_3/La_{0.7}Sr_{0.3}MnO_3$: New Ideas on Spin-Polarized Tunneling, Phys. Rev. Lett. **82**, 4288 (1999).

[21] J. De Teresa, A. Barthelemy, A. Fert, J. P. Contour, F. Montaigne, and P. Seneor, Role of metal-oxide interface in determining the spin polarization of magnetic tunnel junctions, Science **286**, 507 (1999).

[22] S. Liang, H. Yang, H. Yang, B. Tao, A. Djeffal, M. Chshiev, W. Huang, X. Li, A. Ferri, R. Desfeux, S. Mangin, D. Lacour, M. Hehn, O. Copie, K. Dumesnil, and Y. Lu, Ferroelectric control of organic/ferromagnetic spinterface, Adv. Mater. **28**, 10204 (2016).

[23] J. P. Velev, J. D Burton, M. Y. Zhuravlev, and E. Y. Tsymbal, Predictive modelling of ferroelectric tunnel junctions, npj Comput. Mater. **2**, 16009 (2016).

[24] M. Y. Zhuravlev, R. F. Sabirianov, S. S. Jaswal, and E. Y. Tsymbal, Giant Electroresistance in Ferroelectric Tunnel Junctions, Phys. Rev. Lett. **94**, 246802 (2005).

[25] M. Julliere, Tunneling between ferromagnetic films, Phys. Lett. A **54**, 225 (1975).

[26] J.-H. Park, E. Vescovo, H.-J. Kim, C. Kwon, R. Ramesh, and T. Venkatesan, Magnetic Properties at Surface Boundary of a Half-Metallic Ferromagnet $La_{0.7}Sr_{0.3}MnO_3$, Phys. Rev. Lett. **81**, 1953 (1998).

[27] J. Renard and A.-M. Haghiri-Gosnet, CMR manganites: Physics, thin films and devices, J. Phys. D. Appl. Phys. **36**, R127 (2003).

[28] S. S. Lee, J. H. Kim, S. C. Wi, G. Kim, J. S. Kang, Y. J. Shin, S. W. Han, K. H. Kim, H. J. Song, and H. J. Shin, Photoemission spectroscopy and x-ray absorption spectroscopy study of delafossite $AgTO_2$ ($T = \mathrm{Fe}, \mathrm{Co}, \mathrm{Ni}$), J. Appl. Phys. **97**, 10A309 (2005).

[29] V. Garcia, M. Bibes, L. Bocher, S. Valencia, F. Kronast, A. Crassous, X. Moya, S. Enouz-Vedrenne, A. Gloter, D. Imhoff, C. Deranlot, N. D. Mathur, S. Fusil, K. Bouzehouane, and A. Barthelemy, Ferroelectric control of spin polarization, Science **327**, 1106 (2010).

[30] D. Pantel, S. Goetze, D. Hesse, and M. Alexe, Reversible electrical switching of spin polarization in multiferroic tunnel junctions, Nat. Mater. **11**, 289 (2012).

[31] D. Sun, M. Fang, X. Xu, L. Jiang, H. Guo, Y. Wang, W. Yang, L. Yin, P. C. Snijders, T. Z. Ward, Z. Gai, X.-G. Zhang, H. N. Lee, and J. Shen, Active control of magnetoresistance of organic spin valves using ferroelectricity, Nat. Commun. **5**, 4396 (2014).

[32] R. C. Subedi, R. Geng, H. M. Luong, W. Huang, X. Li, L. A. Hornak, and T. D. Nguyen, Extremely low amplified spontaneous emission threshold and blue electroluminescence from a spin-coated octafluorene neat film, Appl. Phys. Lett. **110**, 053302 (2017).

[33] A. Rajapitamahuni, L. L. Tao, Y. Hao, J. Song, X. Xu, E. Y. Tsymbal, and X. Hong, Ferroelectric polarization control of magnetic anisotropy in $PbZr_{0.2}Ti_{0.8}O_3/La_{0.8}Sr_{0.2}MnO_3$ heterostructures, Phys. Rev. Mater. **3**, 021401(R) (2019).

[34] J. M. López-Encarnación, J. D. Burton, E. Y. Tsymbal, and J. P. Velev, Organic multiferroic tunnel junctions with ferroelectric poly(vinylidene fluoride) barriers, Nano Lett. **11**, 599 (2011).

[35] S. Valencia, A. Crassous, L. Bocher, V. Garcia, X. Moya, R. O. Cherifi, C. Deranlot, K. Bouzehouane, S. Fusil, A. Zobelli, A. Gloter, N. D. Mathur, A. Gaupp, R. Abrudan, F. Radu, A. Barthélémy, and M. Bibes, Interface-induced room-temperature multiferroicity in $BaTiO_3$, Nat. Mater. **10**, 753 (2011).

[36] J. P. Velev, J. M. Lopez-Encarnacion, J. D. Burton, and E. Y. Tsymbal, Multiferroic tunnel junctions with poly(vinylidene fluoride), Phys. Rev. B **85**, 125103 (2012).

[37] T. L. Meyer, A. Herklotz, V. Lauter, J. W. Freeland, J. Nichols, E. J. Guo, S. Lee, T. Z. Ward, N. Balke, S. V. Kalinin, M. R. Fitzsimmons, and H. N. Lee, Enhancing interfacial magnetization with a ferroelectric, Phys. Rev. B **94**, 174432 (2016).

[38] J. D. Burton and E. Y. Tsymbal, Prediction of electrically induced magnetic reconstruction at the manganite/ferroelectric interface, Phys. Rev. B **80**, 174406 (2009).

[39] X. Hong, A. Posadas, A. Lin, and C. H. Ahn, Ferroelectric-field-induced tuning of magnetism in the colossal magnetoresistive oxide $La_{1-x}Sr_xMnO_3$, Phys. Rev. B **68**, 134415 (2003).

[40] J. Heidler, M. Fechner, R. V. Chopdekar, C. Piamonteze, J. Dreiser, C. A. Jenkins, E. Arenholz, S. Rusponi, H. Brune, N. A. Spaldin, and F. Nolting, Magnetoelectroelastic control of magnetism in an artificial multiferroic, Phys. Rev. B **94**, 014401 (2016).

[41] M. Y. Zhuravlev, S. S. Jaswal, E. Y. Tsymbal, and R. F. Sabirianov, Ferroelectric switch for spin injection, Appl. Phys. Lett. **87**, 222114 (2005).

[42] X. Xu, A brief review of ferroelectric control of magnetoresistance in organic spin valves, J. Mater. **4**, 1 (2018).